Inorganic Chemistry

Article

pubs.acs.org/IC

Case of a Strong Antiferromagnetic Exchange Coupling Induced by Spin Polarization of a Mn−Mn Partial Single Bond

Hélène Bolvin*[,†] and Frank R. Wagner[‡]

[†]Laboratoire de Chimie et de Physique Quantiques, IRSAMC, Université de Toulouse III, 118 route de Narbonne, 31062 Toulouse Cédex 04, France

[‡]Max-Planck-Institut für Chemische Physik fester Stoffe, Nöthnitzer Straße 40, 01187 Dresden, Germany

Supporting Information

ABSTRACT: The large antiferromagnetic coupling in the Mn^{IV}−Mn^{IV} bond in the $Li_6Ca_2[Mn_2N_6]$ and $Li_6Sr_2[Mn_2N_6]$ crystals (J = −739 and −478 cm^{-1}, respectively, with $\mathcal{H} = -J\vec{S}_A\cdot\vec{S}_B$) is studied using different theoretical methods: solid-state density functional theory calculations, molecular density functional theory, and post-Hartree−Fock calculations with large embeddings. This magnetic coupling is a challenge for theoretical methods because both correlation and polarization effects are crucial for the correct description of the bond. All methods predict a large antiferromagnetic coupling, but none of the considered methods give a quantitative agreement with the experimental values. The molecular methods, except B3LYP and CASPT2, underestimate the coupling for the calcium compound, while they overestimate it in the strontium compound, within 30%. These methods, on the other hand, strongly underestimate the decrease of the coupling between the two compounds, with the most correlated one predicting the same value for both compounds. The solid-state method overestimates the coupling within 60% but reproduces better their ratio. Analysis of the calculations shows that the magnetic coupling between the local π orbitals is not caused by a direct interaction but by the spin-polarized σ bond.

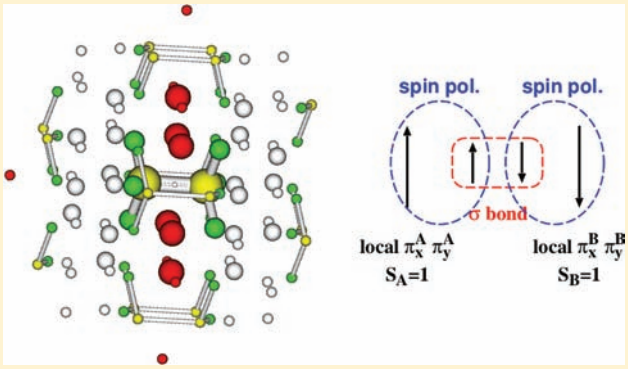

INTRODUCTION

The chemistry of metal−metal multiple bonds was extensively studied in the last decades since isolation of the $[Re_2Cl_8]^{2-}$ anion in the 1960s. Recently, this field has undergone an experimental and theoretical renaissance[1] with the discovery of stable diamagnetic organometallic molecules displaying quintuply $\sigma^2\pi^4\delta^4$-bonded chromium(I) dimers. Although the Cr−Cr distances are extremely short (1.7−1.8 Å), the d_δ orbitals of the weak dd_δ bonds are found to be close to localization such that the effective bond order (EBO)[2,3] calculated at the correlated level of theory is significantly lower than 5. The important role played by the metal−metal distance in general was already analyzed very early:[4] in the$[Cr_2Cl_9]^{3-}$ anion with the structure of a $Cl_3Cr(\mu\text{-}Cl)_3CrCl_3$ confacial bioctahedron, the Cr−Cr distance is 3.12 Å and magnetic data show that there is no Cr−Cr bond because each Cr^{III} ion has three unpaired electrons. In contrast, in the isostructural $[W_2Cl_9]^{3-}$, the W−W distance is much shorter, 2.41 Å, and magnetic data show strong coupling between the local spins such that the assignment of a W−W triple bond is adequate. In these examples, the structure is flexible enough to allow for both scenarios, the mutual avoidance or attraction of the metal centers by axial displacement of the metal atoms in the octahedra apart and toward each other, respectively. The magnetic coupling is discussed entirely in terms of metal−metal interaction, and superexchange mediated by the triple halide bridges seems to be negligible.

In the case of the quaternary nitridomanganates(IV) $Li_6Ca_2[Mn_2N_6]$ and $Li_6Sr_2[Mn_2N_6]$ presented by Kniep et al.[5,6] the Mn_2 units are located within octahedra of nitride anions N^{3-}, forming unsupported Mn^{IV}−Mn^{IV} contacts within ethane-like $[Mn_2N_6]^{10-}$ units with distances d(Mn−Mn) of 2.36 and 2.54 Å for the calcium and strontium compounds, respectively. The electronic structures of these crystalline compounds have been investigated by solid-state density functional theory (DFT) calculations and subsequent analysis of the evaluated electron localization function. It was shown that the Mn−Mn bond should be regarded as a two-center two-electron bond, which makes the compounds the first clear examples of Mn−Mn bonds with Mn in high oxidation state IV +. The fitting of susceptibility curves in terms of a Heisenberg Hamiltonian of the form $\mathcal{H} = -J\vec{S}_A\cdot\vec{S}_B$ with local spins either 1 or $^3/_2$ yields strong antiferromagnetic couplings: in the range 70−700 K, both spin hypotheses yield close but slightly different values of J. The addition of new experimental points in the range 270−1050 K favors the local spin of one with J = −739 cm^{-1} (calcium) and −478 cm^{-1} (strontium), which is

Received: December 19, 2011
Published: June 12, 2012

   dx.doi.org/10.1021/ic2027237 | *Inorg. Chem.* 2012, 51, 7112−7118

consistent with the observed increase of the distance d(Mn−Mn).[7]

These strong antiferromagnetic couplings remind one of those found in bridged Mn^{IV}−Mn^{IV} dimers such as, e.g., $[Mn_2^{IV}(\mu\text{-}O)_3(tmtacn)_2]^{2+}$ (with tmtacn = *N*′,*N*″,*N*‴-trimethyl-1,4,7-triazacyclononane), for which $J = -780\ cm^{-1}$.[8] In a study of the complete series of bridged Mn^{IV} and Cr^{III} with metal−metal distances ranging from 2.3 to 4.0 Å, Wieghardt et al. conclude that the interaction between the two metallic centers is rather due to a direct metal−metal interaction than to a superexchange mechanism.[9] However, subsequent DFT studies of this complex[10−12] conclude either a superexchange[11] or a dominant direct-exchange mechanism.[12]

This work presents a theoretical study of the nature of the coupling between the two Mn^{IV} atoms in the $[Mn_2N_6]^{10-}$ unit using a wide range of methods: starting from BS spin-polarized solid-state DFT calculations, over molecular broken-spin (BS) DFT calculations with embedding, and finally post-Hartree−Fock wave functional theory (WFT) methods are used. The nature of the bond and the mechanism of the coupling will be analyzed and compared to experimental data.

CRYSTAL STRUCTURE DESCRIPTION

The structurally isotypic compounds have been described to crystallize in a variant of the antitype of the La_2O_3 structure with half-filled tetrahedral and octahedral voids: $La_6O_6^{[tet]}O_3^{[oct]} \rightarrow N_6Li_6^{[tet]}Zr_3^{[oct]} \rightarrow N_6Li_6^{[tet]}AE_2^{[oct]}Mn_2^{[oct]}$. In this view, the N atoms form a (distorted) hexagonal close packing (hcp, with layers A and B), where Li atoms occupy all tetrahedral voids (α and β) between every second layer, with the octahedral voids between these layers being empty ($\gamma^{\square}$). Between the remaining layers, the tetrahedral voids are empty ($\alpha^{\square}$ and $\beta^{\square}$) and the octahedral voids (γ) are occupied in a regular fashion by alkaline-earth (AE) atoms (γ^{AE}) and Mn_2 dumbbells (γ^{Mn}) (cf. Figure 1−3), which leads to a 3-fold superstructure of the simple hcp stacking. In the convenient short-hand notation, this complex arrangement can be written as

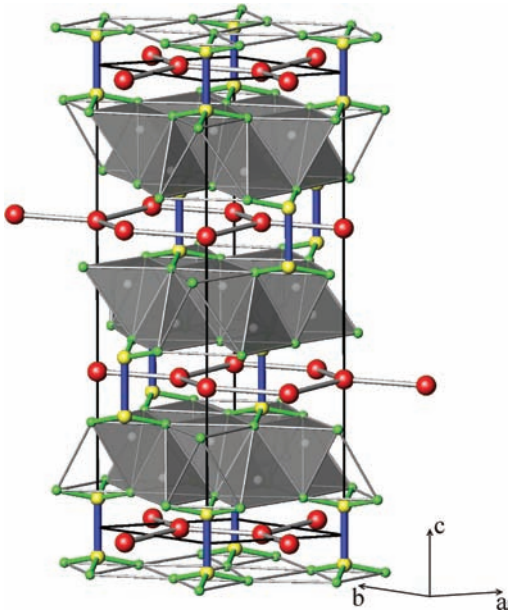

Figure 1. Structure of the $Li_6Ca_2[Mn_2N_6]$ crystal (yellow, Mn; green, N; gray, Li; red, Ca). The unit cell with hexagonal axes containing three formula units is shown in black.

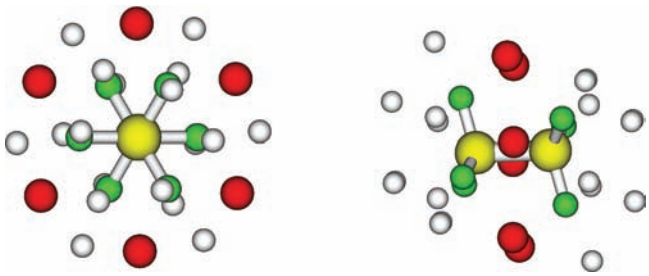

Figure 2. First shell of atoms (yellow, Mn; green, N; gray, Li; red, Ca).

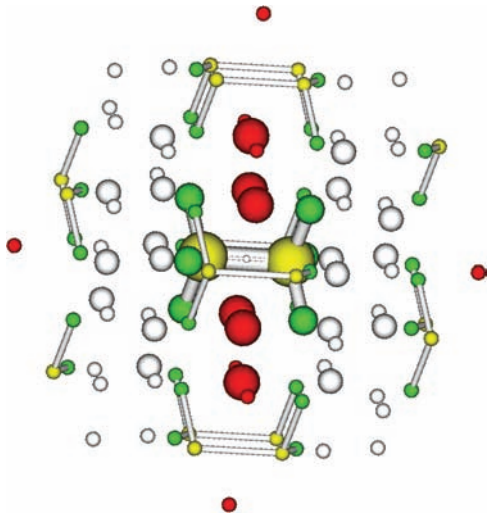

Figure 3. Two first shells of atoms (same colors as those in Figure 2; the ECP is represented with a small radius).

$$A\beta^{Li}\gamma^{\square}\alpha^{Li}B\alpha^{\square}\left(\frac{2}{3}\gamma^{AE}, \frac{1}{3}\gamma^{Mn_2}\right)\beta^{\square}A\beta^{Li}\gamma^{\square}\alpha^{Li}B$$
$$\alpha^{\square}\left(\frac{2}{3}\gamma^{AE}, \frac{1}{3}\gamma^{Mn_2}\right)'\beta^{\square}A\beta^{Li}\gamma^{\square}\alpha^{Li}B\alpha^{\square}\left(\frac{2}{3}\gamma^{AE}, \frac{1}{3}\gamma^{Mn_2}\right)''$$
$$\beta^{\square}A$$

As a result of this arrangement, Mn_2N_6 units are formed, i.e., Mn_2 dumbbells within N_6 octahedra. They are not interconnected by common N atoms. Moreover, also the Mn atoms within the same Mn_2N_6 unit are not connected by common N atoms. Instead, the octahedra centered by Mn_2 dumbbells share common edges with six neighboring ones in the same plane, which are centered by AE atoms. Only these six AE atoms are found in the bridging position. Given the rather rigid behavior of the MnN_3 units [d(Mn−N) stays at 1.80 Å], this explains why the elongation of the octahedra along the trigonal c axis, caused by the larger size of the Sr^{2+} cations (r = 1.18 Å) compared to the Ca^{2+} cations (r = 1.00 Å), leads to an increase of the Mn−Mn distance from 2.36 to 2.54 Å. The respective distances d(AE−N) are 2.52 Å (Ca) and 2.63 Å (Sr) and the shortest distance d(Li−N) = 2.00 Å (Ca) and 2.07 Å (Sr).

Given the experimentally established nonmetallic character of the compounds, the following oxidation states are to be assigned: $(Li^{I+})_6(AE^{II+})_2[(Mn^{IV+})_2(N^{III-})_6]$, with AE = Ca, Sr. Although the Mn_2N_6 units can be considered to be well-separated in terms of covalent interactions, the molecular fragment $[Mn_2N_6]^{10-}$ does not represent a good model for the situation in the crystal because of excessive negative charge.

dx.doi.org/10.1021/ic2027237 | *Inorg. Chem.* 2012, 51, 7112−7118

Besides the delicate electron correlation problem, this introduces a further difficulty for the realistic modeling of the magnetic exchange interaction in the crystalline compounds.

Computational details are given in the Supporting Information.

RESULTS AND DISCUSSION

In the $[Mn_2N_6]^{10-}$ unit, the Mn atoms possess a formal $3d^3$ configuration. The intermetallic axis is taken as the O_z one. The central unit belongs to the $\mathcal{D}_{3d}$ point group, and the orbitals are labeled within this group even if calculations are performed in the C_i group. The scheme of orbitals is depicted in Figure 4.

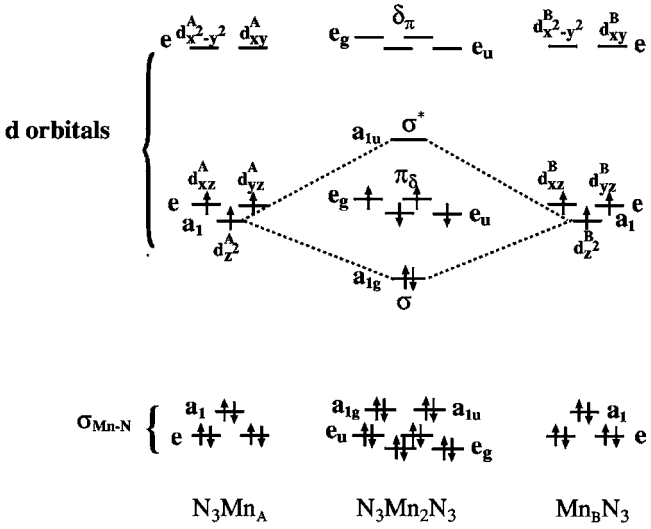

Figure 4. MO scheme.

The two local $d_{z^2}^A$ and $d_{z^2}^B$ orbitals combine to give a bonding σ orbital and an antibonding σ^* orbital of symmetry a_{1g} and a_{1u}, respectively; these orbitals are slightly antibonding with the orbitals of the N atoms. The d_{xz} and d_{yz} orbitals and $d_{x^2-y^2}$ and d_{xy} orbitals belong to the same irreducible representation E and form two sets. One set of hybrids ($\approx^2/_3\delta + {}^1/_3\pi$, denoted as δ_π) forms a bonding interaction with nominal p molecular orbitals (MOs) of the nitrogen ligands, while the other one ($\approx^1/_3\delta + {}^2/_3\pi$, denoted as π_δ) mainly points toward the other metal. The π overlap is tiny, and these orbitals are nonbonding. They are the magnetic orbitals with one nonpaired electron in each of these four π_δ orbitals, denoted as $\pi_{x/y}^A$ and $\pi_{x/y}^B$. With this description, the Mn−Mn bond is a weakened σ bond and the unpaired π electrons form two local spin triplet states that couple to form a singlet, a triplet, and a quintet molecular state of symmetries $^1A_{1g}$, $^3A_{2u}$, and $^5A_{1g}$, respectively. However, because the σ bond is weak, we will additionally consider another spin coupling scheme. In the limiting case, where there is no σ bond, one gets two local quartet spin states that couple to give four magnetic states of symmetries $^1A_{1g}$, $^3A_{2u}$, $^5A_{1g}$, and $^7A_{2u}$.

SOLID-STATE CALCULATIONS

Densities of states (DOSs) have been calculated for the two crystals, in the ferromagnetic and antiferromagnetic configurations. The results for $Li_6Ca_2[Mn_2N_6]$ are shown in Figures 5 and 6. The resulting DOSs display a clear band gap that is consistent with the gaps determined by diffuse reflection of 1.2 eV (1.1 eV) for the calcium (strontium) compound.[7] Below the

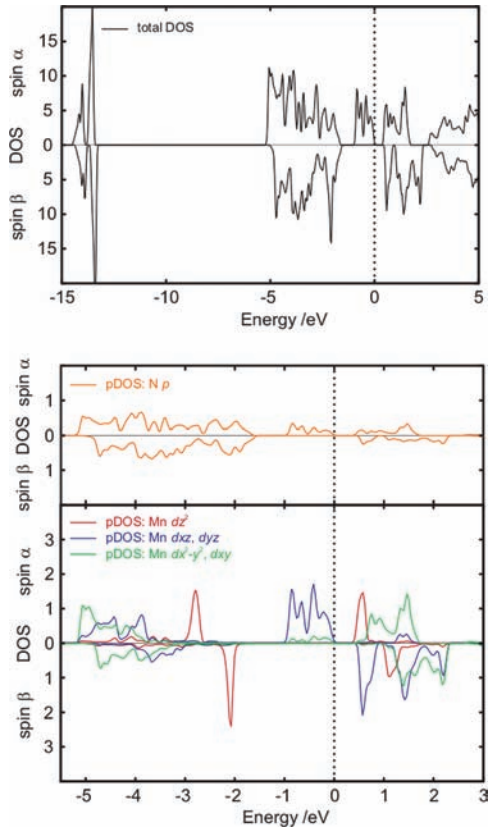

Figure 5. DOS of the ferromagnetic phase of $Li_6Ca_2[Mn_2N_6]$: upper, total DOS; lower, projected.

Fermi level (set to 0 eV), one can recognize three separate DOS structures. The energetically lowest one originates from N(2s) states, which mix only weakly with metal states. The middle one contains two different features, namely, (i) the bonding combinations of nominal N(2p) states with Mn(3d) (π_δ and δ_π) states at lower energies and (ii) the Mn−Mn bonding Mn($3d_{z^2}$) states. The corresponding σ-antibonding combination with opposite spin is located above the Fermi level. Finally, just below the Fermi level, the Mn($3d_{xz}$) and Mn($3d_{yz}$) states are found: the intraatomic mixing of the latter with $d_{x^2-y^2}$ and d_{xy} states seems to be significantly smaller than that in the molecular calculations, but it has to be kept in mind that the projection of atomic orbital character is performed only within the atomic spheres such that the more localized states will get emphasized. In addition to this intraatomic hybridization, some interatomic mixing with N(2p) states is indicated as well. The Mn−Mn bond displays a noticeable spin polarization; the α population of $3d_{z^2}$ is larger than the β one on site 1. The resulting total magnetic moments per unit cell (with two Mn atoms) for the antiferromagnetic and ferromagnetic calculations are 0.0 and 4.0 μ_B, respectively. The antiferromagnetic solution is more stable than the ferromagnetic one by 2125 cm^{-1} (Ca) and 1620 cm^{-1} (Sr) per Mn_2 dimer. One deduces that $J = -1063$ cm^{-1} (Ca) and -810 cm^{-1} (Sr), which are 44% and 69%, respectively, too high in magnitude. Thus, the increase of the distance d(Mn−Mn) from 2.36 to 2.54 Å is calculated to be accompanied by a decrease of the antiferromagnetic stabilization of 24%. This is in fair agreement with the experimental results, where the decrease is 35%. It is to be noted that the overshooting of the experimental values corresponds to an overestimated

dx.doi.org/10.1021/ic2027237 | Inorg. Chem. 2012, 51, 7112−7118

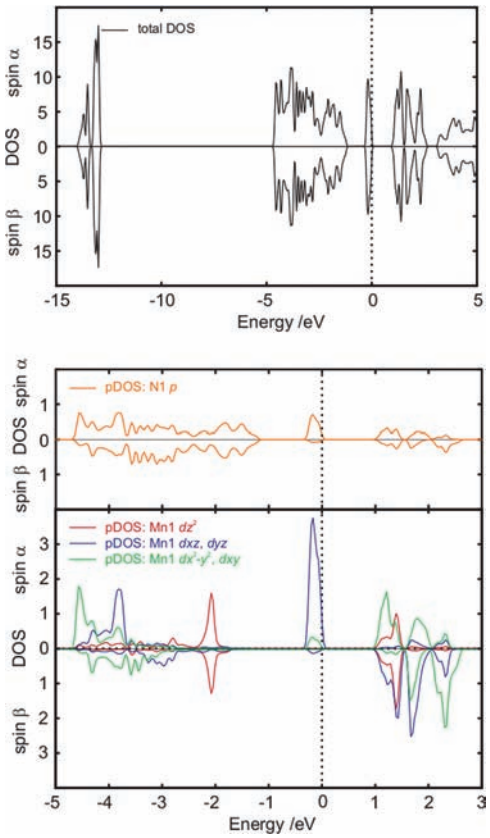

Figure 6. DOS of antiferromagnetic $Li_6Ca_2[Mn_2N_6]$ performed in the BS approach: upper, total DOS; lower, projected on sites N1 and Mn1 (the DOS projected on N2 and Mn2 is obtained by inversing the α and β densities).

delocalization, i.e., too high degree of ddπ_δ bonding, of the magnetic orbitals due to correlation defects in the functional. As an empirical cure, the introduction of a Hubbard U parameter in the framework of the local-density approximation + U method addresses this issue. For sure, a value of U could be found that leads to a much better agreement with experiment, but this was not the goal of this work.

MOLECULAR DFT CALCULATIONS

The results for the unrestricted DFT calculations on the embedded Mn_2N_6 units are summarized in Table S1 in the Supporting Information. Generalized gradient approximation (GGA) functionals BLYP and PBE give results in good agreement with experimental data, but the hybrid B3LYP overestimates the couplings and, even worse, does not reproduce the tendency between the two compounds with a smaller coupling for the calcium compound than for the strontium one. The energy of the determinant with $M_S = 3$ is very high: it confirms that the σ interaction must be considered as a bond, and the magnetic scheme is the coupling between two local spins of one. The high-spin (HS) and BS states are respectively described by the determinants $|HS\rangle = |\sigma\bar{\sigma}\pi_x^A\pi_y^A\pi_x^B\pi_y^B|$ and $|BS\rangle = |\sigma'\bar{\sigma}''\pi_x^A\pi_y^A\bar{\pi}_x^B\bar{\pi}_y^B|$, where σ is a symmetrical combination of the local σ^A and σ^B orbitals and σ' and σ'' swerve toward sites A and B, respectively. Because σ has a weight of 44% on the two d_{z^2} orbitals, the bond is partial. The polarization of the σ' and σ'' orbitals induces a large spin polarization of the σ bond; in the BS state, the spin population in the $3d_{z^2}$ orbital is 0.23 (Ca) and 0.28 (Sr) electrons with the PBE functional. This analysis shows that the σ bond is partial and spin-polarized.

The decrease of the J couplings calculated with BLYP and PBE between the calcium and strontium compounds is 19%.

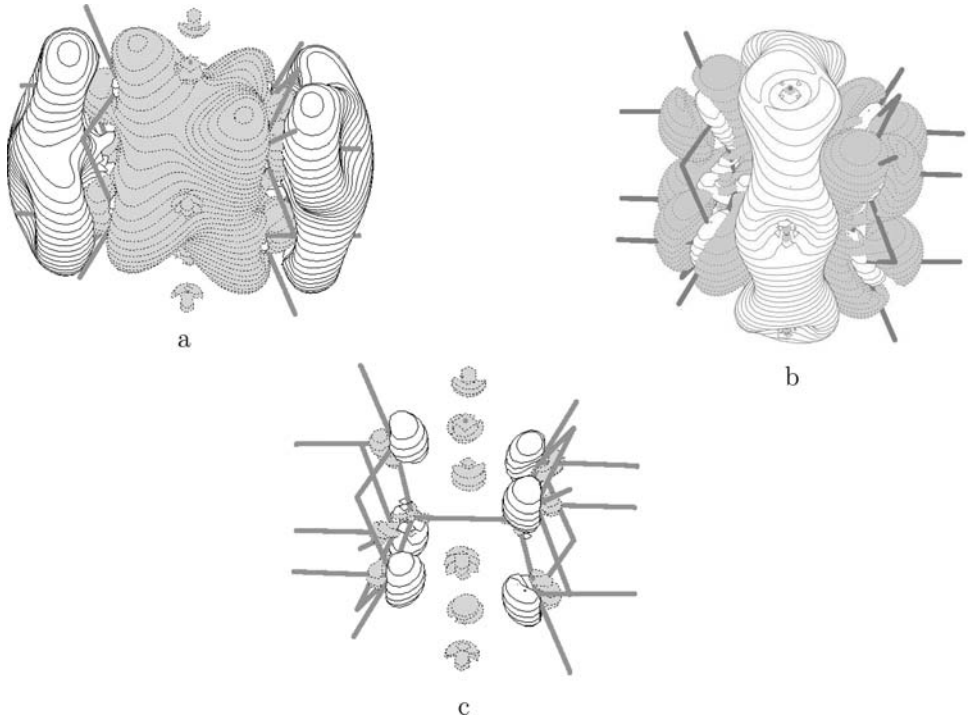

Figure 7. Differential charge density obtained with CASSCF(6,6) with different levels of description of the Ca^{2+} atoms. The reference is the description using the basis set: (a) nothing; (b) point charges 2+; (c) ECP.

dx.doi.org/10.1021/ic2027237 | Inorg. Chem. 2012, 51, 7112–7118

WFT CALCULATIONS

The Li atoms attract a large part of the electron density because the $[Mn_2N_6]$ unit has a formal charge of 10−. According to Mulliken charges, it effectively bears a charge of 4−, while there is a transfer of 6 electrons to the 18 Li^+ cations. The effect of the Ca cations on the metal−metal bond can be analyzed by changing their description. We have compared five different levels of description for the Ca^{2+} cations, namely, (i) skipping them, (ii) point charges, (iii) an ECP without basis set, (iv) basis set, and (v) full embedding. The results are summarized in Table S2 in the Supporting Information. Difference density maps of the total electron density with respect to case iv are given in Figure 7. There is virtually no charge transfer between the N atoms and Ca^{2+} cations, but these cations exert an important electrostatic influence on the Mn−Mn bond region. When they are omitted, there is a lack of electron density in the zone of the Mn−Mn bond and a large excess on the Li atoms, with one of them becoming almost neutral. In the presence of point charges, the effect is opposite; the electron density is overestimated in the Mn−Mn region. Neither of these two descriptions is faithful even if the spin density is quite good and the spin gaps between magnetic states are quite correct. The main effects of the calcium are qualitatively well-described by pseudopotentials: the electron density is stabilized in the Mn−Mn region by electrostatic attraction with the 2+ charges, and the large volume of Ca cations confines this density close to the Mn−Mn axis.

The EBOs calculated with the quintet CAS(6/6)SCF wave function are 0.48 and 0.39 for the calcium and strontium compounds, respectively. The σ bonding is halfway between a covalent bond and a magnetic system. The EBO of the σ bond increases to 0.75 for the calcium compound with a higher level of correlation (CAS+S, CAS+DDCI2, and CAS+DDCI3). The energy gaps calculated by CASPT2 and DDCI are summarized in Table S3 in the Supporting Information. CAS(4/4)CI considerably underestimates J. In this calculation, the σ orbital is doubly occupied, and there is no correlation; this shows that the direct coupling between the π magnetic orbitals is negligible. Once the σ orbitals are included in the active space, one gets the correct order of magnitude for the magnetic coupling; the σ bond plays the key role in the interaction. CASPT2 does not give good results. The larger the active space, the worse is the agreement with the experiment, and the CASSCF results are better than the CASPT2 ones. Configuration interaction (CI) calculations are performed with the more symmetrical cluster, without embedding. CAS(6/6)-S calculations performed with and without embedding are very close; this shows that the embedding does not provide any effect on the metal−metal region. CI methods give better results. The monoexcitations increase J, and the diexcitations decrease it. For calcium, J is underestimated by 12, 5, 10, and 28% at the CASCI, CAS-S, CAS-DDCI2, and CAS-DDCI3 levels, respectively, while for strontium, J is overestimated by 10, 31, 26, and 11%, respectively. While CASCI values show a decrease from calcium to strontium, the DDCI3 values are almost the same for the two compounds, with the strontium value being even slightly larger. A common feature of the correlation is to consistently increase the energy of the sextet state, which is due to the strengthening of the σ bond by inclusion of the correlation. The projection of the wave function in the active space is strongly altered by the correlation. This should be the reason why CASPT2 does not properly treat the correlation in these systems because this method is a contracted one, in the sense that it does not reoptimize the projection of the wave function within the active space. When the CI wave functions have been expressed in terms of the local orbitals $\sigma^{A/B}$ and $\pi^{A/B}_{x/y}$, the determinants dominating the singlet wave function are $|\sigma^A\pi^A_x\pi^A_y\bar{\sigma}^B\bar{\pi}^B_x\bar{\pi}^B_y|$ and $|\bar{\sigma}^A\bar{\pi}^A_x\bar{\pi}^A_y\sigma^B\pi^B_x\pi^B_y|$, where the three spins localized on the same center are parallel. The weight of these determinants is double compared to the $|\bar{\sigma}^A\pi^A_x\pi^A_y\sigma^B\bar{\pi}^B_x\bar{\pi}^B_y|$ and $|\sigma^A\bar{\pi}^A_x\bar{\pi}^A_y\bar{\sigma}^B\pi^B_x\pi^B_y|$ ones (0.47 versus 0.23 at the CASCI level). This shows that the σ bond is polarized: the $\sigma\alpha$ spin orbital comes close to the center with the $\pi\alpha$ spin density and, similarly, the $\sigma\beta$ spin density comes close to the $\pi\beta$ one.[13−15] This denotes the strong spin polarization of the σ orbitals that was already evidenced in the solid-state and molecular DFT calculations. The coupling scheme between the two local spins is depicted in Scheme 1. The π orbitals are local

Scheme 1. Spin Coupling Scheme

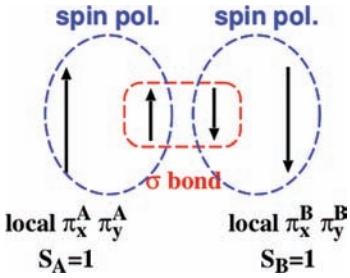

and do not interact directly. The local Hund rule favors a local parallel alignment of the two "π electrons" with the "σ ones". The σ orbitals form a covalent bond; they are delocalized and antiparallel, but this bond is significantly spin-polarized. This conclusion is consistent with the conclusions made by Hochrein[7] but analyzes the mechanism underlying the antiferromagnetic coupling. The antiferromagnetic coupling of the π orbitals is carried by the σ orbitals. The model Heisenberg Hamiltonian $\mathcal{H} = -J\vec{S}_A\cdot\vec{S}_B$ with two local spins of one fulfills the Landé rule, $\Delta E_{ST} = -J$ and $\Delta E_{SQ} = -3J$. The CI results fulfill this rule within 15%; this shows that these magnetic systems can be described by the indirect coupling of local π orbitals.

The main difference between the two compounds is the metal−metal distance, with d(Mn−N) being unchanged. The molecular calculations do not correctly reproduce the decrease of the magnetic coupling between the two compounds. In order to analyze the effect of the metal−metal distance, the cluster has been deformed, keeping the distances unchanged in the two subblocks MnN_3Li_9. Calculations are performed in the $\mathcal{D}_{3d}$ cluster without embedding. The Ca cations placed in the median plane do not move. The results are shown in Figure 8. While CASSCF energy gaps decrease very rapidly with the distance, the CASPT2 behavior looks odd, especially the large increase of the singlet−quintet gap around 2.7 Å, but it has already been noted that the CASPT2 results are not faithful for this system. The CI results show a plateau: DDCI gaps do not depend on the distance between 2.5 and 3 Å. The BLYP results show a small increase around 3 Å; we do not have the results for distances larger than 3 Å because the calculations did not converge at large distances. The presence of this plateau can be understood: upon an increase in the distance, the EBO of the σ bond decreases, correlation effects become more important, and the breaking of the bond makes the spin polarization of this

dx.doi.org/10.1021/ic2027237 | Inorg. Chem. 2012, 51, 7112−7118

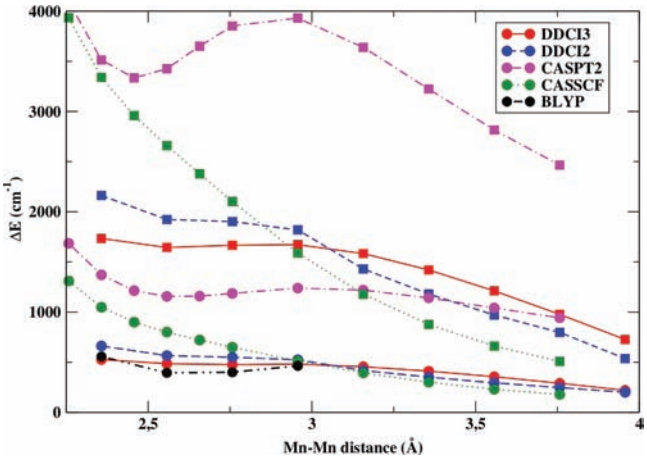

Figure 8. Singlet−triplet ΔE_{ST} (circles) and singlet−quintet ΔE_{SQ} (squares) gaps versus metal−metal distance. All calculations are performed with CAS(6/6) on the $\mathcal{D}_{3d}$ cluster.

bond more efficient. This shows that the indirect interaction between the π orbitals is important even for quite large metal−metal distances. It seems that all of the correlated cluster approaches fail to reproduce the decrease of the magnetic coupling with the metal−metal distance found experimentally, while the solid-state calculation manages it better. This is surprising because, in this crystal structure, the magnetic Mn_2N_6 units are well-separated and long-range ordering is expected only at very low energy scales. The comparison between the solid-state and cluster DFT calculations using the same functional shows that the former strongly overestimate $|J|$ but give the best ratio J_{Ca}/J_{Sr} while the latter give values of J closer to the experimental ones, but with a nonsystematic error because one is overestimated and the other is underestimated and the ratio is much too small. In this case, the solid-state and cluster approaches are not consistent with each other. CI calculations give values of J on the same order of magnitude as the cluster calculations using GGA functionals, but the ratio J_{Ca}/J_{Sr} decreases with the level of correlation. Hybrid functionals and CASPT2 do not give valuable results.

CONCLUSIONS

In the two crystals $Li_6Ca_2[Mn_2N_6]$ and $Li_6Sr_2[Mn_2N_6]$, one finds a Mn^{IV}−Mn^{IV} bond with a very strong antiferromagnetic coupling, J = −739 and −478 cm^{-1}, respectively. Solid-state calculations have been performed on the whole crystal and compared to the cluster approach where the $[Mn_2N_6]^{10-}$ unit is embedded in three shells of ions, with the first shell being described by full basis sets. All calculations reproduce the large antiferromagnetism of these two compounds (see Table 1).

Table 1. Experimental and Calculated Magnetic Coupling Constants (cm^{-1})

	$-J_{Ca}$	$-J_{Sr}$	J_{Ca}/J_{Sr}
exp	739	478	1.55
PBE (crystal)	1063	810	1.31
PBE	723	606	1.19
BLYP	642	518	1.24
B3LYP	1165	1414	0.82
CAS(14/14)PT2	1494		
MR-DDCI3	529	533	0.99

The decrease of the coupling between the two crystals is correctly described by the solid-state method, but the values of J are overestimated. Solid-state and molecular PBE results are not equivalent, although there is no magnetic coupling between the dimers and there is no 3D ordering in the considered crystals. The cluster approach predicts the correct order of magnitude within 30% for the couplings except B3LYP and CASPT2; the decrease is underestimated by all methods and is even zero with DDCI3, which is supposed to be the most accurate method used in this work. The magnetic coupling is systematically underestimated for $Li_6Ca_2[Mn_2N_6]$ and overestimated for $Li_6Sr_2[Mn_2N_6]$. The correct description of the metal−metal bond in these two compounds is clearly challenging for the methods of quantum chemistry because it combines four localized electrons, a weak bond, and strong dynamical correlation effects that affect the zeroth-order wave function.

All methods evidence the strong spin polarization of the σ bond. The Mn−Mn interaction consists of a weakened (EBO < 0.5) σ bond supplemented by four unpaired π electrons. The π orbitals do not interact directly but through the delocalized spin-polarized σ orbitals. A more detailed study of the mechanism of interaction will be published in a forthcoming publication. The strength of the coupling reminds us of the interaction in tri-μ-OMn^{IV} dimers in which there is still a controversy over whether the magnetic coupling is due to a direct or superexchange interaction. After the conclusions of this work, one may ask whether the interaction there could not also be, at least partially, direct through the σ bond.

ASSOCIATED CONTENT

Supporting Information

Computational details including solid-state and molecular calculations and tables of energy gaps, of a comparison of the description of Ca atoms, and of a difference of energies calculated by CASSCF, CASPT2, and DDCI. This material is available free of charge via the Internet at http://pubs.acs.org.

AUTHOR INFORMATION

Corresponding Author

*E-mail: bolvin@irsamc.ups-tlse.fr.

Notes

The authors declare no competing financial interest.

ACKNOWLEDGMENTS

The authors thank Walter Schnelle, Vincent Robert, Jean-Baptiste Rota, Nathalie Guihéry, and Jean-Paul Malrieu for fruitful discussions.

REFERENCES

(1) Wagner, F. R.; Noor, A.; Kempe, R. *Nat. Chem.* **2009**, *1*, 529.
(2) Hall, M. B. *Polyhedron* **1987**, *6*, 679.
(3) Roos, B. O.; Malmquist, P.-A.; Gagliardi, L. *J. Am. Chem. Soc.* **2006**, *128*, 17000.
(4) Cotton, F. *Rev. Pure Appl. Chem.* **1967**, *17*, 25.
(5) Hochrein, O.; Grin, Y.; Kniep, R. *Angew. Chem., Int. Ed.* **1998**, *37*, 1582.
(6) Hochrein, O.; Höhn, P.; Kniep, R. *Z. Anorg. Allg. Chem.* **2003**, *629*, 923.
(7) Hochrein, O. Ph.D. Thesis, 2001, http://elib.tu-darmstadt.de/diss/000156/.
(8) Wieghardt, K.; Bossek, U.; Nuber, B.; Weiss, J.; Bonvoisin, J.; Corbella, M.; Vitols, S. E.; Girerd, J. *J. Am. Chem. Soc.* **1988**, *110*, 7398.

(9) Niemann, A.; Bossek, U.; Wieghardt, K. *Angew. Chem., Int. Ed.* **1992**, *31*, 311.
(10) Zhao, X. *Inorg. Chem.* **1997**, *36*, 1198.
(11) Delfs, C. D.; Stranger, R. *Inorg. Chem.* **2000**, *39*, 491.
(12) Pantazis, D. A.; Krewald, V.; Orio, M.; Neese, F. *Dalton Trans.* **2010**, *39*, 4959.
(13) Clotet, A.; Daudey, J. P.; Malrieu, J. P.; Rubio, J.; Spiegelman, F. *Chem. Phys.* **1990**, *147*, 293.
(14) Guihéry, N.; Malrieu, J. P.; Evangelisti, S.; Maynau, D. *Chem. Phys. Lett.* **2001**, *349*, 555.
(15) Malrieu, J. P.; Guihéry, N.; Calzado, C. J.; Angeli, C. *J. Comput. Chem.* **2007**, *28*, 35.